# 4

# Integrated Assessment of GW Decline through Gravimetric Remote Sensing and Field Observations

## 4.1 INTRODUCTION

The baseflow in the arid and semi-arid regions is sustained by GW discharge into rivers and streams, especially during dry periods when surface runoff is minimal. Its relationship with GW is crucial for effective water resource management since GW levels significantly maintain baseflow. The high hydraulic gradient due to enhanced GW levels between the river and GW enhances the baseflow. Conversely, when GW levels drop due to over-extraction or drought, less GW is available to feed into SWs, decreasing baseflow. Additionally, GW's recharge and discharge dynamics (determined by factors such as precipitation, infiltration, and water withdrawal) control the long-term availability of GW for baseflow. The characteristics of the aquifer itself, such as its permeability and hydraulic connectivity, further influence how much GW contributes to baseflow.

Before implementing measures to manage baseflow, conducting a thorough GW assessment is essential. This assessment provides insights into GW availability, natural recharge rates, and current GW trends. Without understanding the state of the GW system, efforts to enhance baseflow may be ineffective. GW assessments also help identify critical areas where recharge can be enhanced or where excessive GW abstraction needs to be controlled. GW assessment is also necessary to ensure the long-term sustainability of baseflow management measures. Some interventions, such as artificial recharge, directly impact GW levels and must be planned carefully to avoid unintended consequences like

waterlogging or salinization. Additionally, continued over-exploitation of GW without assessing GW trends could undermine any short-term success in increasing baseflow.

GW has been important in India's socioeconomic development, serving as the principal drinking water supply and irrigation. However, rising population pressures and the consequences of climate change have greatly reduced the availability of this vital resource, resulting in a downward trend in GW storage (GWS) (Tiwari et al., 2009). This decrease in GW levels has reduced the interaction between river systems and aquifers, notably in major rivers (Das et al., 2021a, 2021c; Mukherjee et al., 2018), harming both riverine ecosystems (Malard et al., 2002) and water quality (Yang et al., 2020). As a result, it is critical to collect precise information on the geographical and temporal distribution of water resources to permit optimal management of both surface and GW systems (Tao et al., 2023).

A precise volumetric evaluation of water across different storages across the hydrological cycle is necessary for the effective management of water resources. Including important hydrological elements like rainfall, evapotranspiration, soil moisture, runoff, GW recharge, GW storage, pumping, and leakage to streams, this entails quantifying the spatial and temporal variations in surface and GW resources (Ahi and Cekim, 2021; Yihdego and Khalil, 2017). However, topographical restrictions like inaccessibility and spatial heterogeneity, as well as economic considerations like the expenses of installation, observation, and maintenance, make it difficult to estimate these characteristics, particularly when high-resolution data is needed.

Remote sensing has emerged as the most cost-effective and efficient way to monitor hydrological variables across wide areas (Hakeem et al., 2021; Li et al., 2022). It provides substantial prospects for water resource monitoring and data assimilation, especially in

remote areas, with consistent observations at regular intervals (Tao et al., 2023). The Gravity Recovery and Climate Experiment (GRACE) satellite mission launched in 2002 was a significant step forward in estimating GW storage anomalies (GWSA). GRACE allowed for the calculation of GWSA essentially as the residual of observed water fluxes or by integrating both observed and modeled fluxes (Humphrey et al., 2023), whereas previous techniques relied on highly precise observed hydrological fluxes and models (Hirschi and Seneviratne, 2017). GRACE gave the first direct observations of terrestrial water storage anomalies (TWSA), delivering monthly anomalies relative to a baseline (2004 – 2009) on a grid scale of 30km *30km.

Despite its revolutionary capabilities, GRACE's spatial resolution is insufficient for extensive hydrological study at the basin level. To overcome this, several methods have been developed to downscale GRACE-TWSA data to smaller resolutions, such as data assimilation and model-based downscaling (Claire Pascal et al., 2022). Data assimilation techniques use high-resolution auxiliary data, such as the Normalized Difference Vegetation Index (NDVI) and MODIS-observed evapotranspiration (MODIS-ET), to develop regression models that forecast GRACE-TWSA at smaller scales (Ahi and Cekim, 2021; Arshad et al., 2022). Furthermore, simulated hydrological variables from physically based land surface models, such as the Global Land Data Assimilation System (GLDAS), are used as inputs for training regression or machine learning models to generate high-resolution TWSA data (Chen et al., 2023; Pulla et al., 2023; Wang et al., 2023). Machine learning approaches are being used to improve TWSA estimates (Sabzehee et al., 2023; Tao et al., 2023; Yin et al., 2022a, 2022b; Zhong et al., 2021).

GRACE-TWSA data, combined with Global Land Surface Model outputs, has been extensively used in large-scale investigations to determine GW storage (GWS) and its anomalies (Srivastava and Dikshit, 2022; Sun, 2013; Vishwakarma, 2020). The simulated

hydrological variables from GLDAS, such as soil moisture (SMS), canopy water storage (CWS), snow water equivalent (SWE), and surface runoff (Qs), are used to derive GWS trends from GRACE-TWSA (Jing et al., 2020; C Pascal et al., 2022; Srivastava and Dikshit, 2022). These advances have significantly improved our ability to monitor and manage GW resources with greater precision and accuracy.

Hydrometeorological variables from the Famine Early Warning Systems Network Land Data Assimilation System (FLDAS) have strong correlations with GRACE-derived Terrestrial Water Storage Anomalies (GRACE-TWSA), allowing GRACE-TWSA to be downscaled to 1 km resolution (Khorrami et al., 2023). Local hydrological models also show a strong association with observed precipitation, a fundamental driver of TWSA, making precipitation critical for validating downscaled TWSA in tropical locations (Kalu et al., 2024; Yin et al., 2022a). Precipitation additionally influences the simulation of hydrological variables in models (Neitsch et al., 2011). Apart from the global scale hydrological model, a local watershed model, such as the Soil and Water Assessment Tool (SWAT)(Arnold, J. et al., 2012), has never been used for downscaling GRACE data.

SWAT has been designed to accurately simulate hydrological variables and streamflow at the watershed scale, offering high levels of parameterization and multivariate calibration (Du et al., 2013; Rajat and Athira, 2021; Yang et al., 2008). It is extensively used to model both overland processes and streamflow routing, including nutrient transport across land and water systems. SWAT's integration with other models—such as MODFLOW for combined surface and GW modeling (Preetha et al., 2021; Tewari et al., 2023), global climate models for predicting hydrological fluxes (Gaur et al., 2023), and GRACE data for canal operation analysis (Arshad et al., 2022) —has enhanced the accuracy of hydrological variable estimation. However, combining SWAT with GW flow models remains a challenging process despite its necessity for comprehensive water resource

management. The integration introduces additional parameters, increasing uncertainty and necessitating more observational data for proper calibration.

Global hydrological models such as GLDAS provide time-based estimates of Terrestrial Water Storage (TWS) and related variables. However, these estimates often have inaccuracies, which make them unsuitable for directly measuring hydrological parameters at the basin scale. To address this issue, GRACE-derived Terrestrial Water Storage Anomalies (GRACE-TWSA) are used to adjust for these inaccuracies by optimizing the differences between GRACE-TWSA and GLDAS-TWSA (Kalu et al., 2024; Khorrami et al., 2023). Once the inaccuracies are corrected, GW storage (GWS) is calculated from the adjusted TWS. This calculated GWS is then used in GW budgeting to identify regions experiencing water stress.

Artificial Neural Networks (ANN) have been widely used in various research areas due to their significant accuracy, particularly in GW potential zonation (Sameen et al., 2019; Tamiru and Wagari, 2022), simulation-optimization (Bahrami et al., 2016), downscaling GRACE-TWSA (Seyoum and Milewski, 2017), climate model outputs (Nourani et al., 2018), and climate variable prediction (Abhishek et al., 2012). ANN's ability to capture complex patterns and nonlinear relationships makes it effective for generating detailed estimates during downscaling (Rogers and Dowla, 1994). However, downscaling accuracy heavily relies on the quality of training data and chosen network architecture (Kumar et al., 2021). Effective data management and optimized network architecture are crucial for robust performance (Vulpe-Grigorasi and Grigore, 2021). While ANN has been integrated with the SWAT model for hydrological simulations and climate model downscaling (Ghaith and Li, 2020; Pradhan et al., 2020), it has not yet been applied to downscale GRACE data using SWAT HRU variables as independent inputs.

A comprehensive methodology for integrated water resource management has been presented. It involves using the SWAT model to assess GW availability and the GWS. The GWS is calculated by refining the GLDAS-TWS data using an Artificial Neural Network (ANN) model with GRACE-TWSA. This improved estimation of GW Storage is then downscaled to the HRU level using another ANN model, which utilizes the simulated hydrological variables of the SWAT model of the Lower Middle Ganga Basin (LMGB). The main objectives of this research are as follows:

I. Determination of GWS using GRACE-TWSA
II. Downscaling of GWS to HRU level with ANN and determination of its trend
III. Determination of GW level and its trend with downscaled GWS
IV. Assessment of water budgets at the administrative area level (Block)

## 4.2 DATASETS USED IN THE STUDY

We utilized various data streams, such as satellite observations, model outputs, and ground-based observational data, to downscale GRACE-derived GWS to HRU-GWS. Details of the data used in the current study are provided below and summarized in **Table 4.1**.

### 4.2.1 GRACE-TWSA

Terrestrial water storage (TWS) is the sum of all surface and subsurface water, including soil moisture, GW, root zone soil moisture, snow/ice, river water, lake water, and vegetation storage (Girotto and Rodell, 2019). GW storage is represented as GWS, snow water equivalent as SWE, land ice as LIS, canopy water as CWS, water as soil moisture as SMS, and water available as SW as Qs. The expression for TWS is:

$$TWS = GWS + SWE + LIS + CWS + SMS + Qs \quad 4.1$$

The Gravity Recovery and Climate Experiment (GRACE) has been monitoring the Total Water Storage Anomalies (TWSA) since 2002 by measuring the time-varying anomalies in the Earth's gravity (Humphrey et al., 2023). After the end of its science mission in October 2017, the GRACE Follow-On (GRACE-FO) has been collecting the TWSA data. The GRACE-TWSA provides vertical estimates of monthly anomalies relative to the short-term TWS baseline (Jan 2004 - Dec 2009) at each location, with a spatial resolution of 330 km × 330 km. The monthly JPL-mascon (Mass concentration blocks) TWSA product is provided with a resolution of 0.50 × 0.50 (≈55 km), although the effective resolution is 30 × 30. The product has been corrected for Glacial Isostatic Adjustment (GIA) and ocean/land leakage, so it does not require additional filtering or signal leakage correction (Save et al., 2016; Vishwakarma, 2020). The JPL-mascon data has shown less residual in the long-term trends for the Ganga River Basin compared to CSR-mascon data as well as the CSR Tellus gridded spherical harmonics rescaled data (Scanlon et al., 2016). Although the CSR-mascon data has a higher resolution than JPL-mascon, it underestimates the decreasing trends of TWSA in the Ganga River Basin, and hence, we used the JPL-mascon data in this study.

### 4.2.2 GLDAS outputs

The GLDAS (Global Land Data Assimilation System) is designed to produce accurate fields of land surface states and fluxes. It achieves this by integrating both satellite and ground-based observational data with advanced land surface modeling and data assimilation techniques (Rodell et al., 2004). Another key aim of GLDAS is to refine the

model's accuracy through data assimilation, which incorporates satellite-based observations and is further supported by ground-based measurements. In this context, the study focuses on utilizing components of the water balance, including surface and subsurface storage (SMS, CWS, Qs), to downscale and accurately estimate GW storage (GWS).

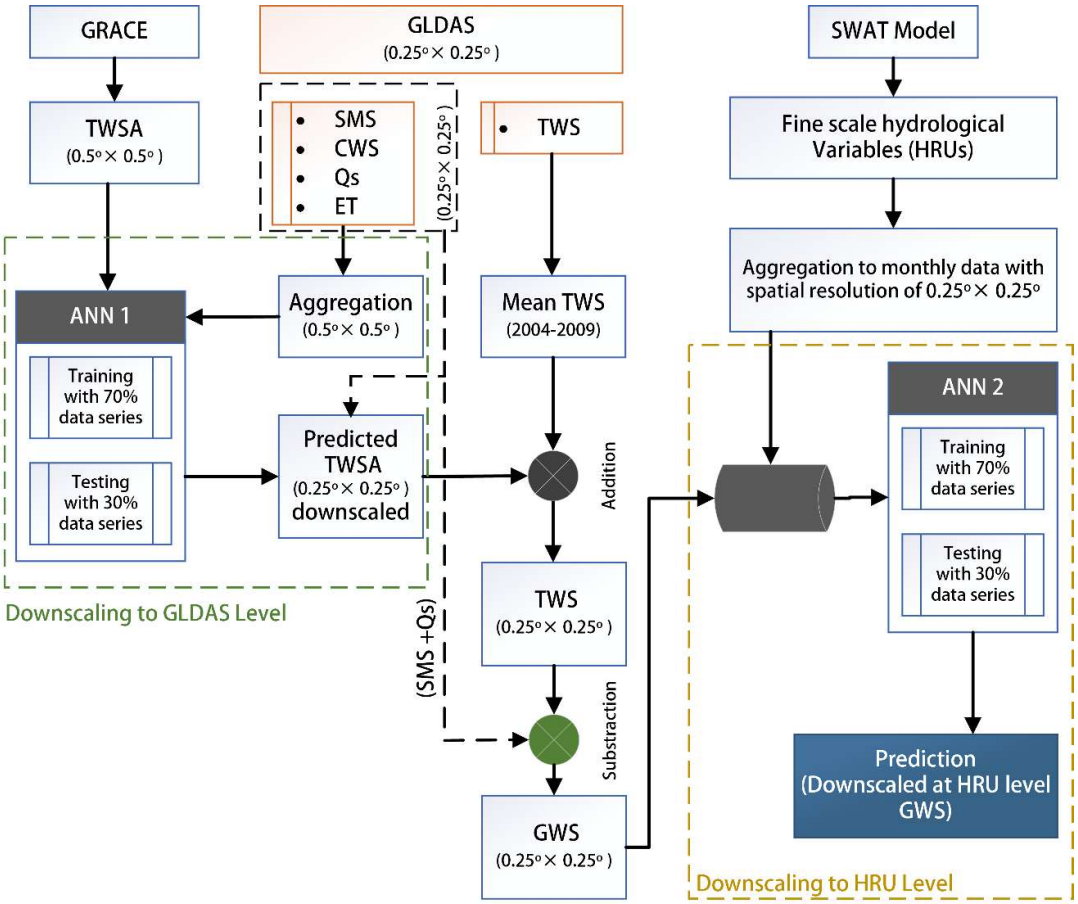


***Figure 4.1****.Methodology flow chart for the determination of HRU-scale GWS*

### 4.2.3 Environmental variables

To downscale the GWS to HRUs scale, predictors used include the nine outputs of the SWAT model with a correlation greater than 0.5. These variables have a direct correlation

with GW storage, either as a source (*PRECIPmm, PERCmm, DA_RCHmm*) or as a sink (*PETmm, REVAPmm, SURQ_CNTmm, GW_Qmm, WYLD_Qmm*). The spatial resolution for HRUs ranges from 0.75 $km^2$ to 480 $km^2$. For the initial downscaling of the GRACE TWSA to a 0.25° spatial resolution, soil moisture (*SMS*), plant canopy SW (*CWS*), and storm surface runoff (*Qs*) from the GLDAS outputs were selected based on their significant Pearson correlation coefficients. These independent environmental variables serve as predictors for the ANN model.

### 4.2.4 Ground-based Measurements

We gathered GW level data before and after the monsoon season from 257 monitoring wells in Uttar Pradesh and Madhya Pradesh between 2001 and 2012. Since direct comparison between GRACE-derived GWSA and water level fluctuations is not feasible, we computed GW level anomalies relative to the short-term baseline (average GWL for the years 2004 to 2009), similar to GWSA.

$$GWLA_i = GWL_i - \overline{GWL} \tag{4.2}$$

Where *GWLA* is the GW level anomalies at time step *i* and $\overline{GWL}$ is the short-term average (2004-2009). The anomaly in the downscaled GWS with respect to the baseline has been compared to the GWLA to assess their correlation. The GWLA has also been utilized to calculate the Specific yield ($S_y$) by robust optimization. River discharge data from two gauging stations (Prayagraj and Varanasi) has been collected from the Central Water Commission. The data has been utilized for the inlet discharge data for the upstream watershed and calibration of the SWAT model.

**Table 4.1**. Summary of data used in the study.

| Type | Product | Spatial and (temporal) resolution | Period | Source |
|---|---|---|---|---|
| TWSA | GRACE (JPL-RL06.1_v03) | 0.5° × 0.5° (monthly) | 2002–2019 | *https://grace.jpl.nasa.gov/data/get-data/jpl_global_mascons* |
| SMS, CWS, Qs, GWS, TWS | GLDAS | 0.25° × 0.25° (daily) | 2002–2022 | *https://disc.gsfc.naa.gov/datasets* |
| Precipitation | IMD 2D Gridded | 25 km × 25 km (daily) | 1998–2014 | *(Pai D.S. et al., 2014)* |
| Temperature | IMD 2D Gridded | 0.5° × 0.5° (daily) | 1998–2014 | *(Pai D.S. et al., 2014)* |
| Elevation | SRTM | 30 m × 30 m | -- | *http://www2.jpl.nasa.gov/srtm/* |
| GW level (GWL) | Ground-observations | Stations (Seasonal) | 2003–2019 | *Central GW Board and Uttar Pradesh GW Board* |
| Soil types | FAO | Polygons | -- | *https://data.apps.fao.org/map/catalog/srv/eng/catalog.search#/metadata/b47d2800-713c-4cd9-bd34-016161ef806e* |
| River Discharge | Observations | monthly | 2003 - 2014 | *Central Water Commission, India* |
| Reservoir Volume | Observations | monthly | 2009 - 2014 | *https://indiawris.gov.in/wris/* |
| Evapotranspiration | MODIS ET | 500m × 500m (8 days) | 2003 - 2014 | *https://appeears.earthdatacloud.nasa.gov/* |
| Land use | LANDSAT 8 | 30 m × 30 m | 2005 | *https://earthexplorer.usgs.gov/* |

### 4.2.5 Ancillary data

The soil parameters in the SWAT model were obtained from the FAO Soil database. The land use data was derived from Landsat 8 multi-spectral images using the random forest classification algorithm. The area was classified into major land use classes (water body, agricultural area, vegetation, barren land, and built-up area) for SWAT simulation. Calibration datasets included the measured river flow, MODIS 8-day cumulative evapotranspiration, and observed reservoir dynamic storage volume. Five subbasins were

selected across the study area, and mean monthly evapotranspiration data was sourced from "AppEEARS" (**Table 4.1**).

## 4.3 STUDY AREA

The lower middle Ganga basin from Prayagraj to Varanasi has been taken as the study area (**Figure 4.2**). It ranges from 80.46° E to 83.12° E and 24.12°N to 25.66°N, covering an area of 25668 $Km^2$. Apart from the Ganga, the area is covered by two major tributaries- Tons and Varuna River. Tons has the most significant watershed area, around 17535 $Km^{2,}$ while the Varuna River covers 3346 $Km^2$ of the basin area. The area is covered by a high density of low-order streams, providing adequate drainage to the Ganga River during storm events. The primary land use is agriculture, which covers 68.5 % of the study area. The Vindhyan rock is underlain by fertile alluvium. The forest covers 12.6 % of the land, mainly limited to the hilly areas in Mirzapur, Satna and Rewa districts. 8.9 % of the area is either bare soil or barren land.

The geology of the study area can be broadly divided into Alluvium and Vindhyan groups. The north part of the area (Varanasi, Jaunpur, Sant Ravidas Nagar, northern part of Mirzapur and Prayagraj) contains quaternary alluvium consisting of older and younger alluvium, deposited on the weathered bedrock of Vindhyan supergroup. The newer alluvium mainly consists of clayey sand with Kankar, while the older alluvium is fairly consolidated clay with Kankar and fine to medium sand with some gravel. As we move towards the Southwest, the outcrops of upper Vindhyan become visible, covering the Mirzapur, Rewa, and Satna districts. The Vindhyan group in Mirzapur is represented by fine to medium-grained Kaimur sandstone or quartzite and is highly jointed. In the Satna and Rewa districts, the Vindhyan is overlain by shale.

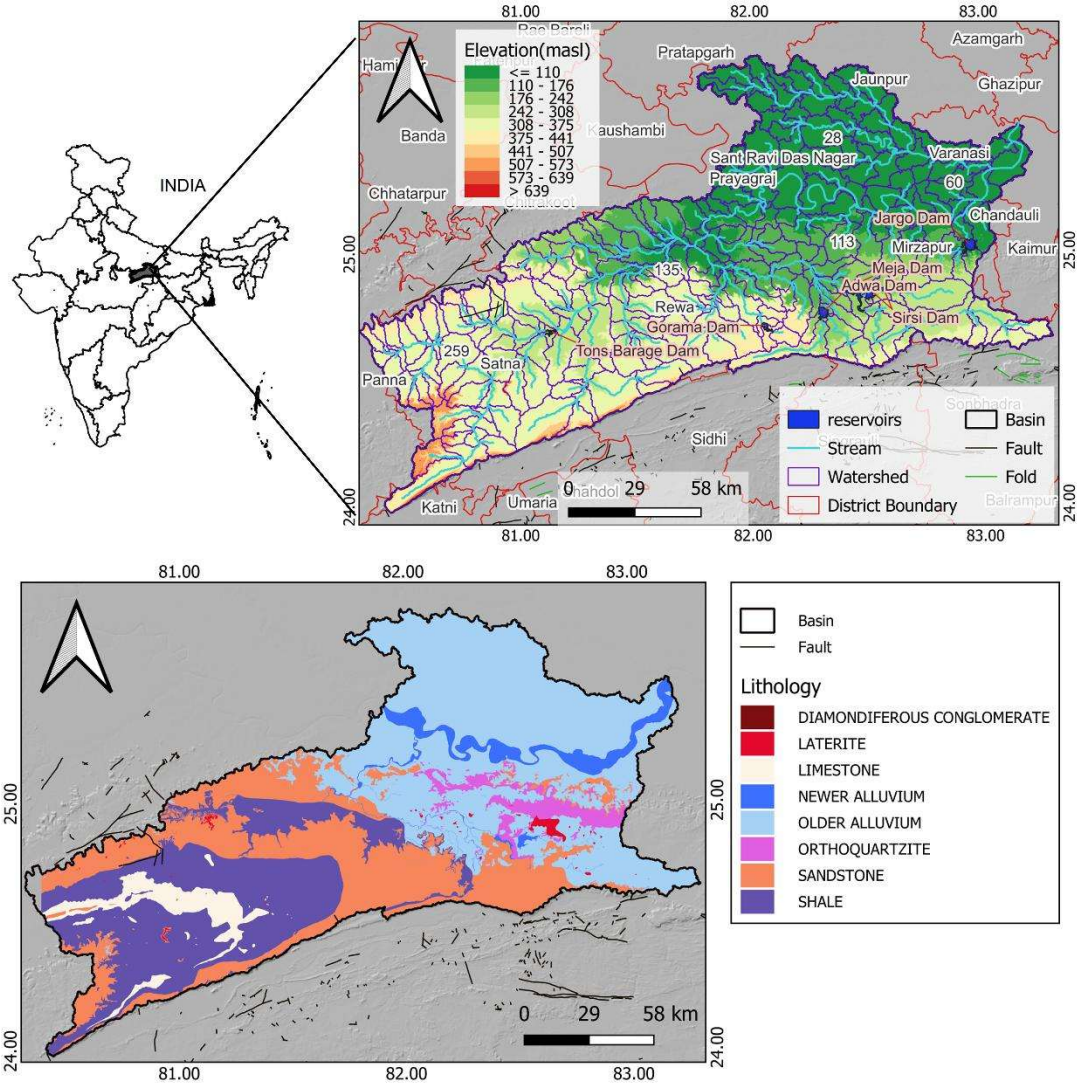


***Figure 4.2**. Study Area with watershed boundaries and stream network (Top) and Lithology (Bottom). The reservoirs and the subbasins (used for set target ET for calibration) is presented as highlighted texts.*

GW occurs within the primary porosity of alluvial sediments; here, the aquifer materials are medium to coarse-grained sand. Shallow aquifers exist in unconfined conditions, whereas deeper aquifers exist in semi-confined and confined conditions. GW in the widely covered Vindhyan Plateau region occurs primarily unconfined within the formation's secondary porosity. However, exploration data suggest that Kaimur sandstone has sufficient GW potential at depths. After the leaching of cementing material, these

sandstones disintegrate and reduce to silica sand, which acts as a promising GW repository. The area covered by shale is found to have reasonable secondary porosity development and a moderate prospect of GW occurrence. In the northern and eastern parts of the Vindhyan region, the aquifers are mainly of an alluvium nature. The GW development practices are mainly limited to the first unconfined and second semi-confined aquifer layers.

The study area can be divided into two parts based on the elevation and climatic conditions: the Vindhyan region and the Gangetic plain. The high-elevated area of Vindhyan, combining parts of Mirzapur, Rewa and Satna, has high annual average rainfall and temperature compared to the low-elevated Gangetic plain. The average annual rainfall observed from 2001 to 2014 in the lower Vindhyan region was 1016 mm, while in the Gangetic plain, it was 829 mm.

## 4.4 DOWNSCALING OF GRACE-DERIVED GWS TO HRU-SCALE

Downscaling GW Storage (GWS) to Hydrological Response Unit (HRU) scale involves a two-stage process. Initially, an Artificial Neural Network (ANN) model addresses the biases in the Terrestrial Water Storage (TWS) data from the Global Land Data Assimilation System (GLDAS) by using data from the Gravity Recovery and Climate Experiment (GRACE) Terrestrial Water Storage Anomalies (TWSA). This correction step adjusts the resolution of TWS data to a finer scale (0.25 degrees).

Following this, the process moves to the second stage, where another ANN model takes over to downscale the corrected GWS data to the HRU scale. This model is specifically trained with various HRU variables, ensuring that the downscaling accurately reflects the local hydrological characteristics at a much finer scale. This method allows for a more

precise and localized understanding of GW resources, essential for effective water resource management.

### 4.4.1 SWAT Model Setup

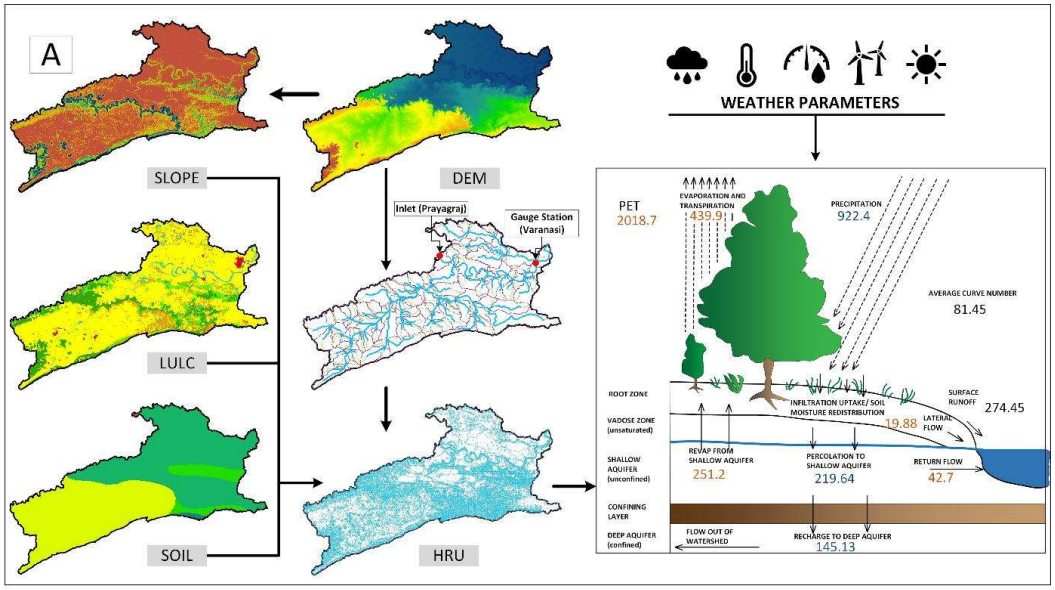


***Figure 4.3.*** *SWAT Model setup and average results for the simulation period of 14 years (2001-2014)*

The SWAT Model has been developed for the 247 km stretch of the Lower Middle Ganga Basin, spanning from the City of Prayagraj to Varanasi, utilizing the ArcSWAT Interface. The watershed and streams have been delineated using a one arc-second (~30-meter resolution) SRTM DEM. A threshold value of 5000 hectares has been employed to define the flow accumulation, resulting in the delineation of 293 watersheds in the basin. The land use, soil, and slope data have been reclassified to determine their unique combinations for HRU delineation (refer to **Figure 4.3**). A total of 1741 HRUs have been defined based on dominant features such as land use, soil, or slope. Weather inputs, including daily rainfall and temperature, have been processed using the weather generator module with IMD 2D gridded data from 1998 to 2014. Additionally, the PET has been calculated using Hargreaves's method (George H. Hargreaves and Zohrab A. Samani,

1985), as it has shown better simulation results in previous studies with available temperature data (Itenfisu et al., 2003). The discharge at the Prayagraj inlet is used as the upstream watershed's discharge into the selected Ganga River reach (**Figure 4.3**).

**Table 4.2**. Reservoir properties (*Source: State Register of Large Dams, Irrigation and Water Resources Department, Uttar Pradesh*)

| S/N | Reservoir | River (Basin) | Surface Area ($Km^2$) | Capacity (MCM) | Seepage coefficient (mm/hr) | Spillway Capacity (cumec) | Full Reservoir Level (masl) | Crest Level of Spillway (masl) |
|---|---|---|---|---|---|---|---|---|
| 1. | Jirgo | Jirgo (Ganga) | 30.72 | 150.85 | 0.71* | 1994.3 | 98.17 | 93.60 |
| 2. | Meja | Belan (Tons) | 4.74 | 300.73 | 0.83* | 11298.0 | 178.04 | 171.91 |
| 3. | Sirsi | Belan (Tons) | 50 | 207 | 0.81* | 2266 | 217.93 | 213.36 |
| 4. | Adwa | Belan (Tons) | 16.67 | 88.1 | 0.74* | 3530 | 195.5 | 185.92 |
| 5. | Tons Barage | Tons | 18.59 | 13.79 | 0.94* | 335.5 | 190.19 | 181.35 |
| 6. | Gorama | Gorma (Tons) | 1. 28 | 3.96 | 0.6* | - | 97.90 | 97.90 |

**Calibrated values*

Before starting the automatic calibration, the seepage coefficient was manually adjusted to align with the stream flow and reservoir volume. The model has identified six main reservoirs, and their properties have been updated in the input files (refer to Table 3). For more information on the detailed modelling approach of reservoirs, please consult the theoretical documentation of SWAT. (Neitsch et al., 2011). The area experiences GW depletion primarily due to irrigation demands (CGWB, 2017). GW serves as the main source of irrigation in the study area (Khan and Singh, 2017). The SWAT management operations include auto-irrigation modeling. In this system, irrigation in a Hydrological Response Unit (HRU) is automatically applied when plant water stress goes beyond a specific threshold value. The deep aquifer is chosen as the irrigation source for each HRU. The model is configured for monthly simulation with a 3-year warmup period.

### 4.4.2 SWAT-Model Calibration

The SWAT model has been calibrated using multiple datasets, including monthly river discharge, monthly reservoir volume, and evapotranspiration. The river discharge at the Varanasi gauge station is the target variable for cumulative flow. The monthly reservoir volume data from the Jirgo dam has been used for calibration. Monthly evapotranspiration has been derived from the 8-day cumulative evapotranspiration product (MOD16) for the five sample subbasins shown in **Figure 4.1**, and these are used as calibration targets (Koltsida and Kallioras, 2022). The Sequential Uncertainty Fitting (SUFI-2) algorithm in SWAT-CUP (Abbaspour, 2019) has been used to calibrate the model with Nash-Sutcliffe efficiency (*NSE*) as the objective function. A total 21 of the most sensitive parameters have been calibrated. The parameter ranks, based on sensitivity, have been presented in **Table 4.3**.

**Table 4.3.** Fitted SWAT Parameters with corresponding sensitivity rank (The method represents the modification performed to the HRU files in each iteration (Replace: Original values have been replaced, Relative: The original values have been multiplied by 1+r where r is the fitted value)

| Rank | Parameter | Method | Minimum | Maximum | Fitted Value | t-stats | p-value |
|---|---|---|---|---|---|---|---|
| 1 | CN2.mgt | Relative | -0.10 | 0.10 | -0.05 | 5.99 | 0.00 |
| 2 | ESCO.hru | Relative | 0.11 | 0.24 | 0.18 | 4.97 | 0.00 |
| 3 | GW_DELAY.gw | Replace | 23.77 | 39.98 | 24.63 | -4.72 | 0.00 |
| 4 | SLSUBBSN.hru | Relative | 0.00 | 0.10 | 0.03 | -2.93 | 0.00 |
| 5 | SOL_AWC().sol | Relative | -0.25 | 1.20 | 0.78 | 2.89 | 0.00 |
| 6 | SOL_K().sol | Relative | 0.00 | 2.00 | 1.44 | -1.30 | 0.19 |
| 7 | GWHT.gw | Replace | 2.00 | 37.21 | 8.38 | 1.16 | 0.25 |
| 8 | RCHRG_DP.gw | Replace | 0.51 | 0.84 | 0.66 | -1.08 | 0.28 |
| 9 | AUTO_WSTRS{..}.mgt | Replace | 0.40 | 0.80 | 0.68 | -1.02 | 0.23 |
| 10 | GWQMN.gw | Replace | 308.72 | 562.78 | 508.75 | -0.98 | 0.32 |
| 11 | GW_REVAP.gw | Replace | 0.07 | 0.21 | 0.17 | -0.89 | 0.37 |
| 12 | GW_SPYLD.gw | Replace | 0.10 | 0.43 | 0.26 | 0.86 | 0.39 |
| 13 | ALPHA_BNK.rte | Replace | 0.56 | 0.93 | 0.62 | 0.77 | 0.44 |
| 14 | ALPHA_BF.gw | Replace | 0.32 | 0.53 | 0.46 | 0.76 | 0.45 |
| 15 | REVAPMN.gw | Replace | 18.12 | 104.20 | 60.63 | 0.68 | 0.49 |
| 16 | HRU_SLP.hru | Relative | 0.01 | 0.05 | 0.01 | -0.45 | 0.65 |
| 17 | OV_N.hru | Relative | -0.09 | -0.02 | -0.06 | -0.35 | 0.72 |

| | | | | | | | |
|---|---|---|---|---|---|---|---|
| 18 | CH_K2.rte | Relative | 0.00 | 2.00 | 0.51 | 0.29 | 0.76 |
| 19 | SURLAG.bsn | Replace | 9.88 | 16.43 | 15.93 | -0.26 | 0.79 |
| 20 | DEEPST.gw | Replace | 13533.45 | 25891.55 | 20912.50 | -0.09 | 0.92 |
| 21 | SHALLST.gw | Replace | 2264.69 | 5008.90 | 4870.50 | -0.01 | 0.99 |

The calibration process is rendered challenging due to uncertainties arising from the utilization of simplified models, the omission of certain processes from the model, and the modeller's lack of awareness of other relevant processes (Abbaspour et al., 2007). The modelling of the specified study area encompasses uncertainties attributable to several factors: (1) the precision of input data, (2) GW extraction for both irrigation and domestic purposes, (3) inherent biases within the observational data, and (4) unidentified processes, including river water abstraction. Furthermore, the calibration process, when reliant on a singular variable, may inadvertently induce biases in alternate hydrological fluxes, thus potentially compromising the model's overall accuracy and reliability (Abbaspour, 2019). The calibration process utilized multiple variables such as river flow, evapotranspiration, and reservoir volume, and the performance was assessed using *NSE* and $R^2$. The fitted parameters demonstrated satisfactory overall performance, as depicted in **Figure 4.4**.

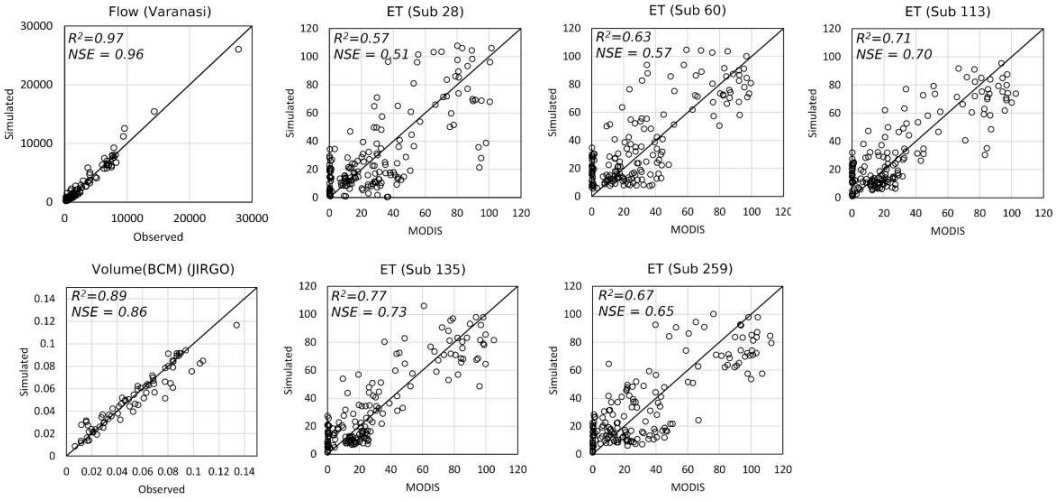


***Figure 4.4**. Scatter plot of observed and simulated values (ET (Sub ##)- Evapotranspiration (mm/month) for the given subbasin)*

### 4.4.3 Calculation of GWS

TWS is a function of other water cycle components (Eq.4.1), which can calculate other components when observed data is available (Rodell et al., 2009). GW Storage (GWS) is a major component of *TWS*, representing the aquifers' available GW. Rearranging the Equation 4.1-

$$GWS = TWS - (SWE + LIS + CWS + SMS + Qs) \quad 4.3$$

The bias in the TWS output of GLDAS has been corrected with downscaled TWSA from GRACE.

$$TWS_i = TWSA_{GRACE,i} + \overline{TWS}_{GLDAS} \quad 4.4$$

Where $TWSA_{GRACE,i}$ represents the downscaled *TWSA* from GRACE to GLDAS resolution at time step '*i*', $\overline{TWS}_{GLDAS}$ is the baseline *TWS* simulated by GLDAS (mean TWS from 2004-2009). The *GWS* was calculated from Eq 4.3 as.

$$GWS_i = TWS_i - \left(SMS_i + Q_{s,i}\right) \quad 4.5$$

The SWE and LIS have been neglected for the study area (semi-arid regions). The CWS is also negligible compared to the GWS. Further, the GWSA has been calculated as

$$GWSA_i = GWS_i - \overline{GWS} \quad 4.6$$

Where $\overline{GWS}$ is the baseline GWS (mean GWS from 2004-2009).

### 4.4.4 Spatial Downscaling with ANN

Utilizing an Artificial Neural Network (ANN) model, the downscaling of Global Water Storage (GWS) to the Hydrological Response Unit (HRU) scale was conducted in two distinct phases. The architecture and hyperparameters of the model were meticulously

selected for each phase and tailored to the dataset in question. For clarity, the ANN models employed in the initial and subsequent phases are denoted as ANN1 and ANN2, respectively. Across both phases, a dedicated model was trained for each large-scale grid, culminating in the training of 22 ANN1 models for the first phase and 65 ANN2 models for the second phase.

In the preliminary phase, ANN1 facilitated the downscaling of GRACE-TWSA to the GLDAS scale, enabling the computation of GWS as per Equation 3.5. The aggregation of predictors from GLDAS was achieved by averaging the GLDAS grids that overlapped with GRACE, subsequently adjusting these to a 0.50 resolution to efficiently train the ANN model (referred to as ANN1 in **Figure 4.1**). Except for the number of neurons (which was varied to optimize accuracy (detailed in **Table 4.4**)). All hyperparameters remained consistent across each grid.

**Table 4.4**. ANN architecture and hyperparameters range (MSE: Mean Squared Error, relu: Rectified Linear Unit)

| Model | Loss function | Activation | Optimizer | No. Hidden Layer | Epoch | No. of Neuron |
|---|---|---|---|---|---|---|
| ANN1 | MSE | relu | adam | 1 | 400 | 2 - 86 |
| ANN2 | MSE | relu | adam | 1 | 200-500 | 2 - 937 |

In the second stage, the GWS was downscaled to the HRUs. The predictors from HRUs have been aggregated to the GLDAS grid by calculating the area-weighted average (Eq. 3.7).

$$var_{HRU,i} = \frac{1}{\sum_j^N A_j} \sum_j^N V_{j,i} A_j \qquad 4.7$$

Where $var_{HRU,i}$ is the value of the HRU predictor at time step *i* (Error! Reference source not found.), N is the number of HRU under the GWS grid ($0.25^0 \times 0.25^0$), $A_j$ is the area of

the *jth* HRU which intersects the GLDAS grid, and $V_{j,i}$ is the predictor value of *jth* HRU at time step *i.* The HRU area intersected by GLDAS grid boundaries has been determined in GIS with the intersect tool. After this, the aggregated predictor HRU variables were prepared and used for model training.

The methodology involved training the ANN2 model by employing aggregated values as the independent variable and GW Storage (GWS) as the dependent variable. For the purpose of optimizing accuracy, adjustments were made to the model's hyperparameters, as depicted in **Figure 4.5**. The accuracy of the model during the training and testing phases was evaluated using the Nash-Sutcliffe Efficiency (NSE) and the coefficient of determination (R2). Subsequently, GWS predictions were made for each Hydrological Response Unit (HRU) within the Global Land Data Assimilation System (GLDAS) grid. For HRUs located on the boundaries of adjacent GLDAS grids, which had been separated during the training phase, GWS predictions were integrated by calculating an area-weighted mean. This integration process involved aggregating the multiple predicted values for common HRUs resulting from predictions made at each grid, utilizing an area-weighted average.

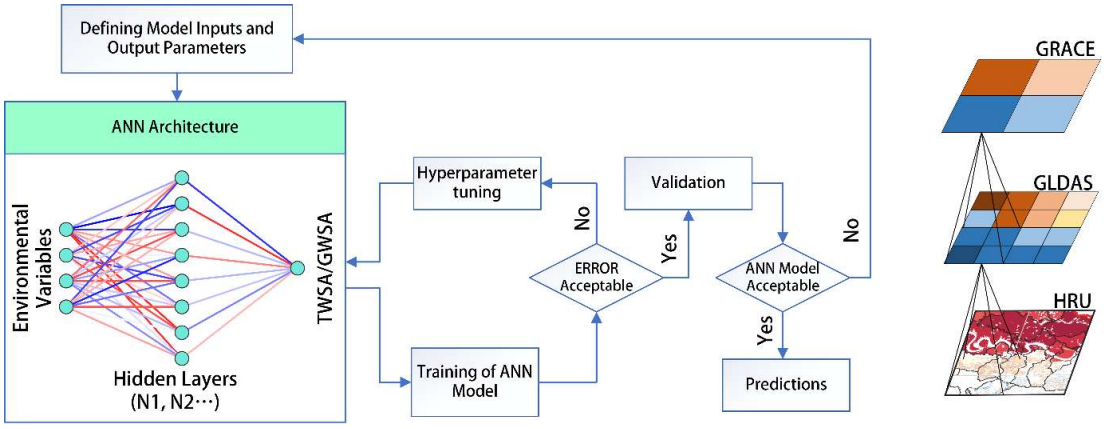


***Figure 4.5****.ANN Model used for downscaling.*

### 4.4.5 Integrated Budgeting of reservoirs in a water cycle

Budgeting water volume within various reservoirs of the hydrologic cycle and its spatiotemporal distribution is crucial for the stakeholders to take suitable interventions. It is vital to assess the long-term effect of constraining discharge and recharge for sustainable GW development (Wiebe et al., 2015; Yihdego and Khalil, 2017). Hydrological models such as SWAT do not parameterize GW reservoir storage and extraction for domestic and industrial water uses, which requires integrating GW flow models (Maxwell et al., 2014). The GW models come with uncertainties in the estimation due to the lack of data on natural variability (Mustafa et al., 2018). The downscaled observed GWS data can aid the water budget estimations to account for GW reservoirs. If the GW storage variation (ΔGWS) is caused by the aquifer recharge and discharge (base flow to streams, GW development (GWD)), the water budget within a zone can be given as -

$$\Delta GWS_i = \sum \left[R_i - (ET_i + Q_{surf,i} + Q_{lateral} + GW\_Q_i + Revap_i)\right] - \sum [GWD_i + BL_i] \quad 4.8$$

Where $R_i$ is rainfall, $BL_i$ is the boundary leakage through the assessment zone, $ET_i$ is evapotranspiration, $Q_{surf,i}$ is surface runoff to the streams, $Q_{lateral}$ is the lateral and return flow to the streams, $GWD_i$ is the GW pumping for irrigation, domestic and industrial use, $GW\_Q_i$ is the base flow to the streams and $Revap_i$ is the amount of GW reaching to vadose zone for transpiration.

Data assimilation based on SWAT outputs and downscaled GWS to equation 4.8 has been utilized to determine the unknown hydrological fluxes in the study area. The hydrological variables (*ET, $Q_{surf}$, $Q_{lateral}$, GW_Q,* and *Revap*) have been taken from the calibrated SWAT model outputs. Further, the GW extraction (*GWD*) for irrigation, industries, and domestic

use has been curated from the NAQUIM Reports (Central GW Board) of all the districts in the study area. The methodology for calculating *GWD* in the NAQUIM Reports cuts through various aspects of observed GW demand from domestic, cattle, irrigation and recreational purposes (CGWB, 2017). The ΔGWS was calculated using the downscaled GRACE data. The block-wise annual average SW and GW budget estimates have been calculated for 75 blocks from 14 districts in the study area. The area-weighted average of SWAT variables was calculated at the block boundary. The unknown boundary leakage from each block has been calculated by rearranging Eq 4.8 as:

$$BL_i = \Delta GWS_i - \sum \left[R_i - (ET_i + Q_{surf,i} + Q_{lateral} + GW\_Q_i + Revap_i)\right] + \sum [GWD_i] \quad 4.9$$

### 4.4.6 GW Sustainability

The human interventions disrupt the natural GW and SW dynamics, which results in GW scarcity in all the storage volumes of the water cycle (**Figure 4.6**). The human interface between the natural hydrologic regime and GW reservoirs shifts the interaction dynamics of these systems (Recharge and Discharge). GW over-extraction for agricultural, industrial, and domestic use leads to significant depletion of aquifers, often exceeding natural recharge rates (Ashraf et al., 2017). Climate change impacts, including increased evapotranspiration and reduced snowmelt, exacerbate GW depletion, especially when combined with over-pumping. The combined effects of climate change and human activities lead to divergent responses in GW storage across different regions, complicating management efforts (Rodell et al., 2018).

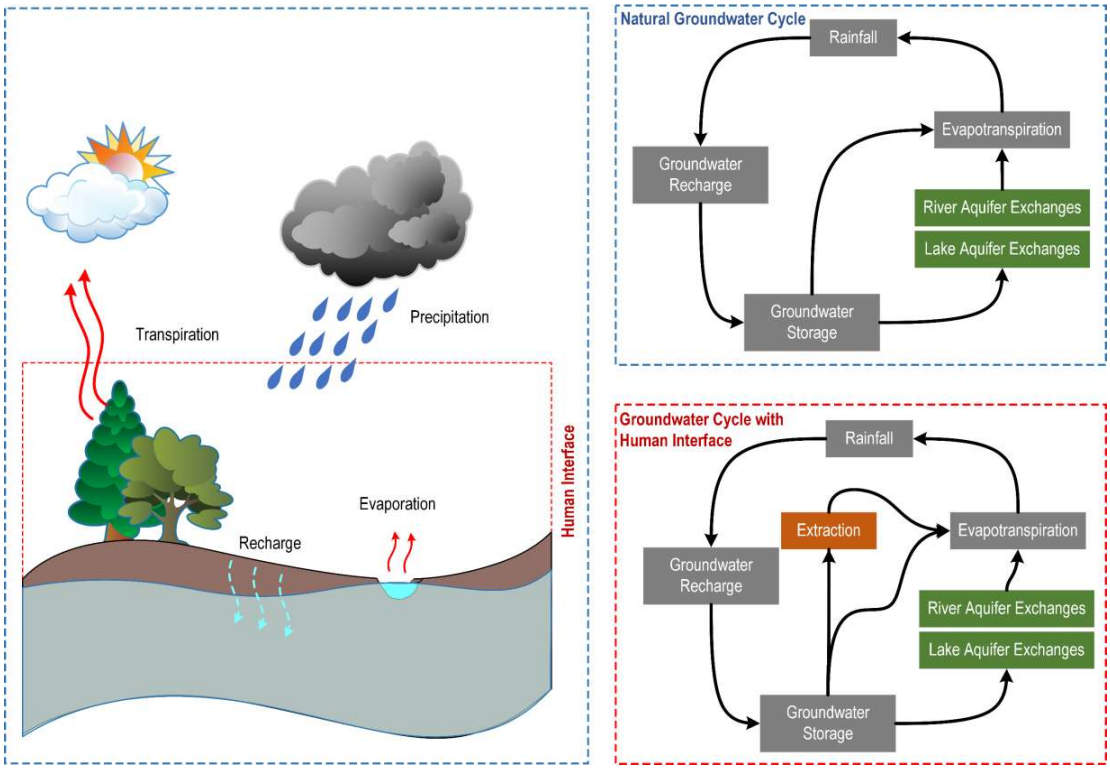


***Figure 4.6***. *Effect of the human interface on the natural GW cycle*

To foster sustainable management of GW resources, it is necessary to assess the stage of over-exploitation in an area. The stage of GW extraction can be assessed by the ratio of net recharge and net discharge from the GW system for an assessment period ($t$) and is given by the GW sustainability ratio (GSR):

$$GSR_t = \frac{R_t - (ET_t + Q_{surf,t} + Q_{lateral,t} + GW_{Q_t} + Revap_t)}{GWD_t} \qquad 4.10$$

Where $R_t$ is rainfall, $ET_t$ is evapotranspiration, $Q_{surf,t}$ is surface runoff to the streams, $Q_{lateral,t}$ is the lateral and return flow to the streams, $GWD_t$ is the GW pumping for irrigation, domestic and industrial use, $GW\_Q_{it}$ is the base flow to the streams and $Revap_t$ is the amount of GW reaching to vadose zone for transpiration. The denominator of Eq 4.10 is calculated by SWAT in the form of net GW recharge (GW_RCHmm). Based on accurate demand data, the GSR can easily be estimated. A GSR greater than 1 indicates

sustainable GW management, a GSR equal to 1 suggests a balanced state and a GSR less than 1 may lead to GW depletion.

## 4.5 RESULTS AND DISCUSSION

### 4.5.1 HRU-based calculation of GWS

To accurately identify high-resolution variations in GW Storage (GWS) within the study area, the research employed Artificial Neural Networks (ANN) to downscale GWS to the level of Hydrological Response Units (HRUs) based on the Soil and Water Assessment Tool (SWAT). The study addressed the bias in Total Water Storage (TWS) observed in the outputs from the Global Land Data Assimilation System (GLDAS) by applying corrections through data obtained from the Gravity Recovery and Climate Experiment (GRACE) Total Water Storage Anomalies (TWSA), subsequently recalculating GWS at the GLDAS resolution. This recalculated GWS was further refined to the HRU level, utilizing SWAT hydrological variables as predictive factors. The degree of this downscaling is inherently reliant on the developed scale of the SWAT model. Notably, the study demonstrates that resolutions as detailed as up to 900 $m^2$ are achievable by selecting a lower threshold for HRU delineation. The precision of the downscaling correlates directly with the resolution of the least detailed input data used in HRU delineation, namely Digital Elevation Models (DEM), land use, and soil data. Moreover, by adjusting the threshold number of cells required for effective flow generation, the methodology allows for the formation of smaller HRUs. However, the research advocates for a methodical approach where a secondary SWAT model is constructed for smaller areas, facilitating a further downscaling of GWS. This approach significantly mitigates computational demands, presenting a scalable and efficient method for detailed GW analysis.

#### *4.5.1.1 HRU Variables and their correlation with GWS*

The predictor variables were chosen based on their correlation with the GWS. The Pearson correlation of all the HRU variables was checked with GWS and among themselves. The variables with the highest correlation with GWS were selected. Since most variables are highly correlated, only one variable from each correlated set was chosen. Nine well-correlated hydrological parameters of SWAT output were selected as the predictor variables in the second stage of downscaling. Seven parameters were positively correlated with GWS, with a correlation coefficient ranging from 0.26 to 0.77. The deep aquifer storage (DA_STmm) had the highest correlation, followed by the deep aquifer recharge (DA_RCHGmm) (coefficient 0.57). The other two parameters showed a negative correlation, with the potential evapotranspiration (PETmm) showing the highest (-0.58) and the "revap" value (water in the shallow aquifer returning to the root zone in response to a moisture deficit (REVAPmm)) showing a minimum of -0.28.

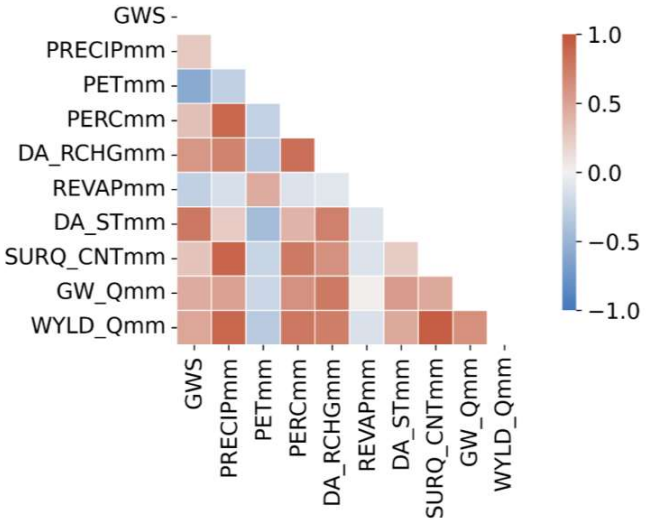


***Figure 4.7.*** *Pearson's correlation between SWAT Parameter and GWS*

The soil water estimates from SWAT are calculated using a water balance approach that considers all significant hydrological variables. This approach showed a strong

correlation with GWS, as illustrated in **Figure 4.7**. The fluctuations in aquifer storage are mainly driven by GW recharge due to precipitation (Scanlon et al., 2012). The region with high GW replenishment is vulnerable to substantial, extended irregularities in the GW storage (GWS). The relative year-to-year variations primarily influence these irregularities in the GWS in the unsaturated zone due to changes in water flow and weather events (Frappart et al., 2019; Swenson et al., 2008). The main factors causing hydrologic changes are climate variables and GW development. Short-term variations are mainly due to excessive GW pumping and flooding. The SWAT model can simulate GW pumping for irrigation purposes, but it does not account for domestic water usage (Neitsch et al., 2011).

The SWAT outputs show spatial heterogeneity, following skewed normal, multi-gaussian, or even no distribution patterns. This makes the downscaling problem suitable for machine learning. Machine learning algorithms are advantageous for mapping the non-linear relationships in the dataset, making them perfect for predicting SWAT outputs, as most parameters have complex nonlinear relationships with hydrological factors (refer to Table 4.2 ). Precipitation is one of the main drivers of the GWSA, followed by ET and GW extraction in the area. The average precipitation in the area varied from 604 mm to 1085 mm during 2001-2014. Rainfall is high in the Vindhyan region. The simulated potential evapotranspiration (PET) is also high in the Vindhyan region due to the high yearly average temperature (**Figure 4.8**).

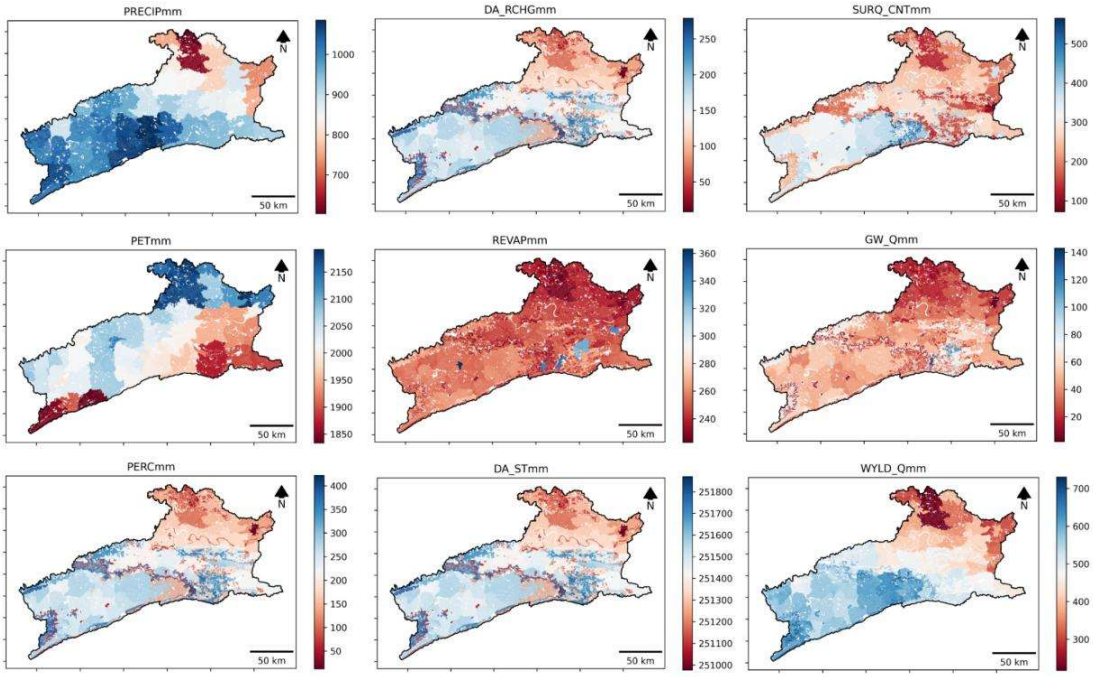


***Figure 4.8**. Yearly mean values of HRU outputs*

### *4.5.1.2 GWS downscaled to HRUs*

The training accuracy for the first stage of downscaling with ANN1 was in the range of NSE: 0.74 to 0.94 and $R^2$: 0.79 to 0.96. The model was validated, and the accuracy was well within the satisfactory range (NSE: 0.81 to 0.95 and $R^2$: 0.80 to 0.95) (**Figure 4.9**. A1-A4). After the downscaling of TWSA to the GLDAS scale, the GWS was calculated. The GWS has been downscaled to HRUs by the ANN2 model trained with the HRU predictors. The training accuracy was in the NSE range of 0.81 to 0.98 and $R^2$: 0.82 to 0.99, while the testing accuracy was found in the NSE range of 0.70 to 0.91 and $R^2$: 0.72 to 0.89 (**Figure 4.9**. B1-B4).

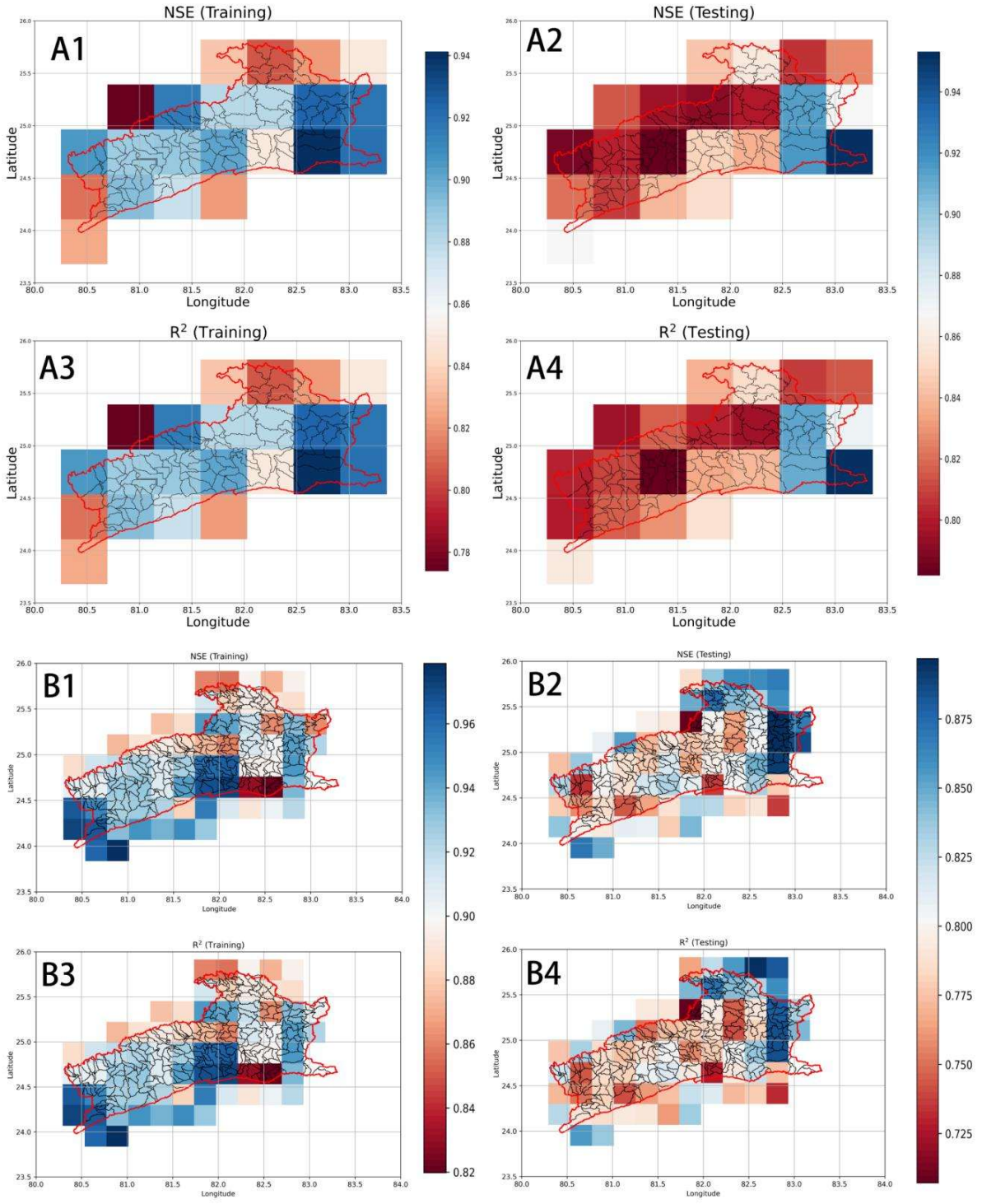


***Figure 4.9***. *Training and testing accuracy of ANN Models (A1-A4. for downscaling of TWSA from GRACE to GLDAS, B1-B4. For downscaling GWS to HRUs)*

The Mann-Kendall test at 95% confidence for GWS at the GLDAS level shows no significant trend for most of the grids inside the study area. Only five grids (two at the eastern and the southern boundary) have shown significant increasing trends of 4.8 mm/year. The maximum decreasing trend of 7 mm/year and maximum increasing trend of 4.8 mm/year have been observed for the grids inside the study area. The overall mean GWS has shown a downward trend of 2.29 mm/year in the study area from 2001 to 2014.

The GWS trend at the 95% confidence level for the downscaled data at the HRU scale was insignificant for 645 HRUs. These HRUs manifest a yearly trend of -1.8mm/year to 2.4mm/year. A total of 786 HRUs show an increasing trend in the range of 1.0mm/year to 6.6mm/year. The remaining 310 HRUs show a decreasing trend in the range of -1.4mm/year to -6.9mm/year. The spatial pattern of GWS has been normalized for comparison, and the GWS trend for the GLDAS and HRU scales is presented in **Figure 4.10**. The Gangetic plain residing on the northern side of the Ganga River has shown a decreasing trend in GWS in the range of -1.4mm/year to -6.9mm/year, while the plain between the foothills of the Vindhyan range and Ganga River has shown mixed trends. The western part of the alluvial plain between the foothills of the Vindhyan range and the Ganga River has shown an increasing trend of up to 6.6mm/year, while the eastern part manifested a decreasing trend of -1.3mm/year. Most of the Vindhyan area (50%) has manifested an increasing trend from 0.9mm/year to 6.1mm/year. About 38% of the Vindhyan area has no significant trend. The remaining 12% of the Vindhyan area has shown a decreasing trend from -1.3mm/year to -3.9mm/year (**Figure 4.10**.B3).

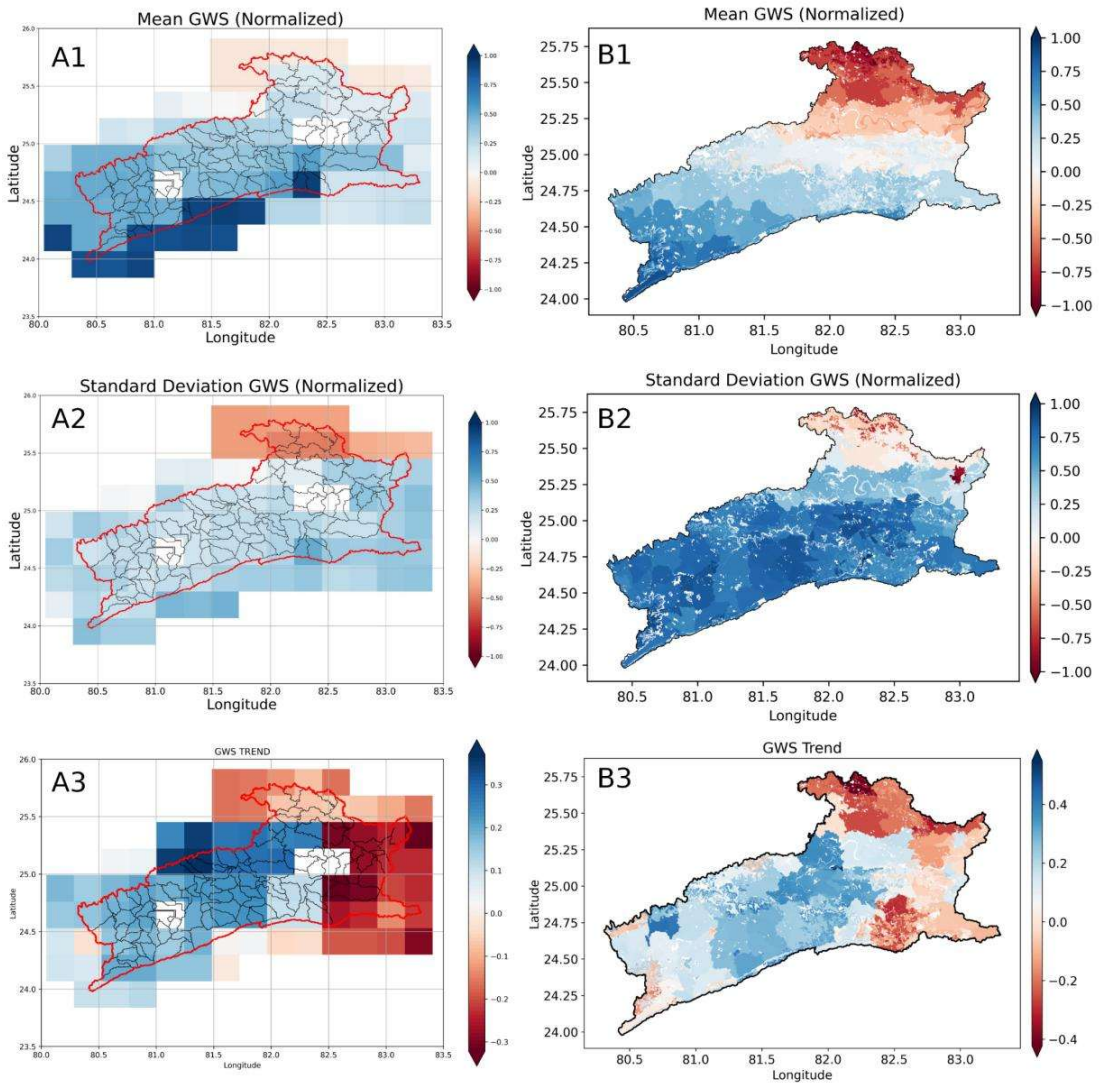


***Figure 4.10****.(A1-B1) Normalized mean GWS at GLDAS and HRU scale respectively, (A2-B2) Standard deviation of GWS on GLDAS and HRU-scale respectively, and (A3-B3) monthly GWS trends for GLDAS and HRU scale respectively.*

The correlation between downscaled GWS and observed GW level from the year 2001 to 2014 has been calculated using the Pearson correlation coefficient (ρ) to validate the downscaling accuracy. Out of 1741 HRUs, the 257 monitoring wells covered only 181 HRUs. The Pearson correlation coefficient for these 181 HRUs was found to be in the range of 0.12 to 0.91, with a mean of 0.6. A total of 124 HRUs have shown a good correlation (ρ>0.5), while 34 HRUs have shown a satisfactory correlation (ρ>0.3). The

correlation analysis represents a satisfactory accuracy since 81.3% of HRUs have shown a good correlation with observed GWL. The GWS variation of four wells (two in Gangetic Plain and two in the Vindhyan region) has been plotted with respect to the observed GWL (**Figure 4.11**). The average monthly precipitation corresponding to the wells in the Gangetic and Vindhyan regions has also been plotted. A similar trend has been observed for the GWL, downscaled GWS and Precipitation in the study area.

### 4.5.2 Determination of GW Level in the HRUs

Determination of the GW level (GWL) is a critical task in GW management due to expensive measurements and inadequate distribution of piezometers, often supplemented by simulated heads from GW models (P. J. Omar et al., 2020). The GRACE-derived GW Storage (GWS) offers an advanced solution to this issue. The GW Level (GWL) is directly linked to GW storage. Ideally, there should be a linear correlation between GWS and GWL, but inadequate model fitting can occur due to observational uncertainty and temporal mismatch between satellite data acquisition and observation times. Additionally, the lack of time series data can also lead to poor model fit (Kumar et al., 2021). Decision tree-based machine learning models are best suited for prediction with scarce datasets (Kumar et al., 2021).

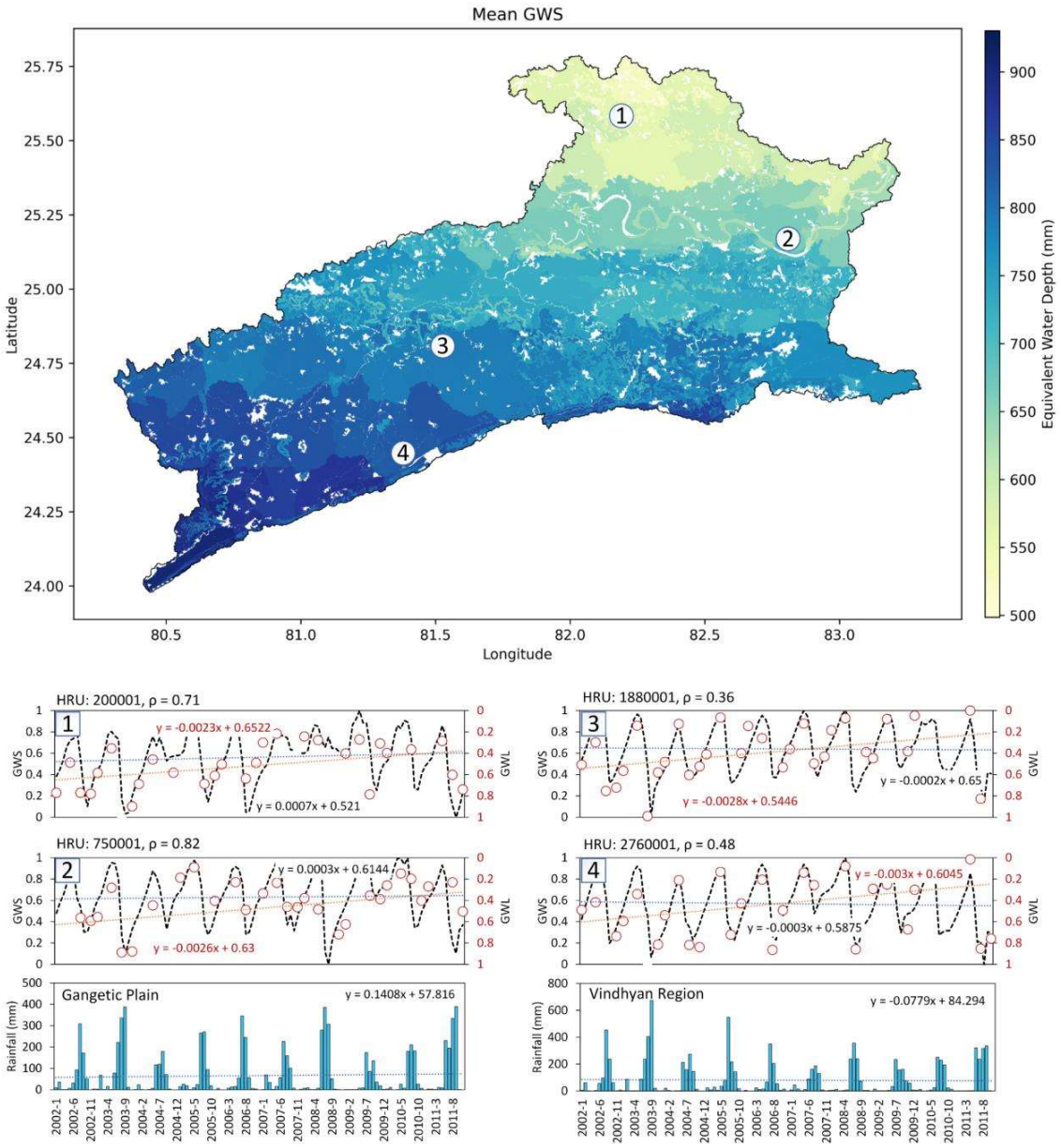


***Figure 4.11***. *The monthly mean of downscaled GWS during 2001-2014 (The temporal variation of GWS for HRUs (1-4) and corresponding GWL observation has been presented along with the correlation coefficient (ρ) and monthly rainfall)*

Here, we utilised the downscaled GWS data and the observed GWL to predict the GW depths over the study area. As the GW is highly influenced by topography (Condon and Maxwell, 2015), GWS, latitude, longitude, and elevation were also selected as the independent variables. Multiple machine learning models (Artificial Neural Networks

(ANN), random forest regressor (RFR)(Breiman, 2001), support vector regressor (SVR), K-nearest neighbour (KNN), and Cat boost regressor (CBR)(Dorogush et al., 2017)) have been tested for the prediction accuracy with *RMSE* and $R^2$. The $R^2$ is sensitive to the data range and can provide false accuracy. Since the standard deviation of the observed GWL is in the range of 0.54 mbgl to 8.3 mbgl (average 2.58 mbgl), which is less when compared to the GW heads (in the range of 60.42 masl to 226.5 masl), the GW depths have been predicted instead of the heads to avoid overestimation of $R^2$. The decision tree-based models (RFR and CBR) have performed better with RMSE of 2.24 ($R^2$:0.76) and 2.16 ($R^2$:0.77), respectively, compared to ANN (RMSE 4.00: $R^2$ 0.23), SVR (RMSE 4.51: $R^2$ 0.12), and KNN (RMSE 4.2: $R^2$ 0.15). The CBR model has been selected for predictions, and its hyperparameters have been tuned to optimum values using grid search. The final RMSE and $R^2$ achieved was 2.06 and 0.8 respectively, with optimal hyperparameters as 'depth'= 6, 'iterations'=1500, 'l2_leaf_reg'= 5 and 'learning_rate'= 0.1.

The overall GW decreases during the pre-monsoon season from 0.04 cm to 8.6 cm per year for 71% of the total area, with a significant contribution from the Vindhyan region, where the trend is high. However, GW replenishment is high in the Vindhyan region compared to the water-stressed Gangetic plain, resulting in an overall increasing trend of GW. The Varanasi, Sant Ravidas Nagar, and Mirzapur districts in the Gangetic Plain have shown a decreasing pre-monsoon GW trend varying from 2.2 cm to 4.6 cm per year. The rest of the study area has shown an increase in water level ranging from 0.01cm to 4.7 cm per year. The area faced approximately 60% of the expected average rainfall from 2004 to 2010. The effect of decreased rainfall can be observed in the GW level in the pre-monsoon (month of May) GWL up to 2011 (**Figure 4.12**).

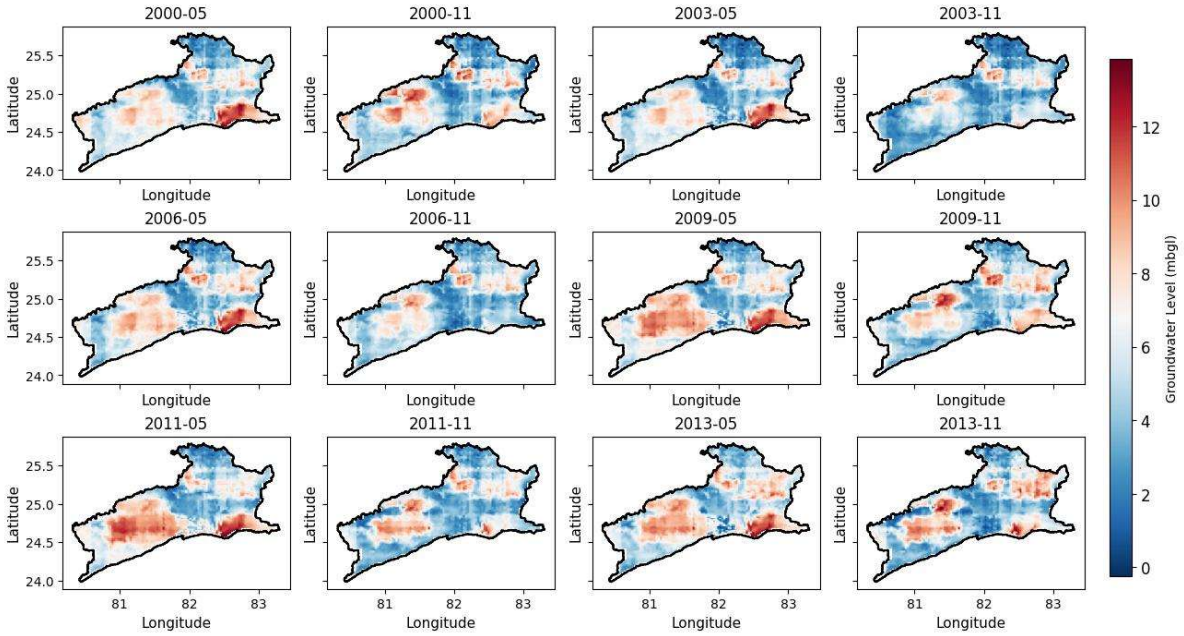


***Figure 4.12.****Predicted pre-monsoon (May) and post-monsoon (November) GW levels from 2000 to 2013.*

### 4.5.3 Mapping the SW and GW Fluxes and GW Sustainability

The net annual GW extraction per unit recharge area is high for the blocks in the Gangetic Plain due to heavy dependency on GW (87.5 %) (Khan and Singh, 2017). Almost all the subbasins are losing their GW reserves in the Gangetic Plain during the assessment period. Out of 33 blocks in the Gangetic alluvium, 12 were on the verge of being GW-scarce regions (GSR $\lesssim$ 1), while the rest were in the critical stage (GSR <1).

Boundary leakage is also high for the regional aquifer system. The negative value of boundary leakage represents gaining conditions such that these subbasins are fulfilling their overdraft from the upstream aquifers, as the regional flow of GW is towards the Ganges River from the northwest direction. The blocks in the Vindhyan region have less GW development, and most of the area is still GW-sufficient (GSR ≥1). The river Ganga separates the two regions based on GW deficiency. The lower part of the Vindhyan region

fulfills the overdraft demand of the lower alluvial plain and further drains into the river Ganges as base flow (Das et al., 2021b).

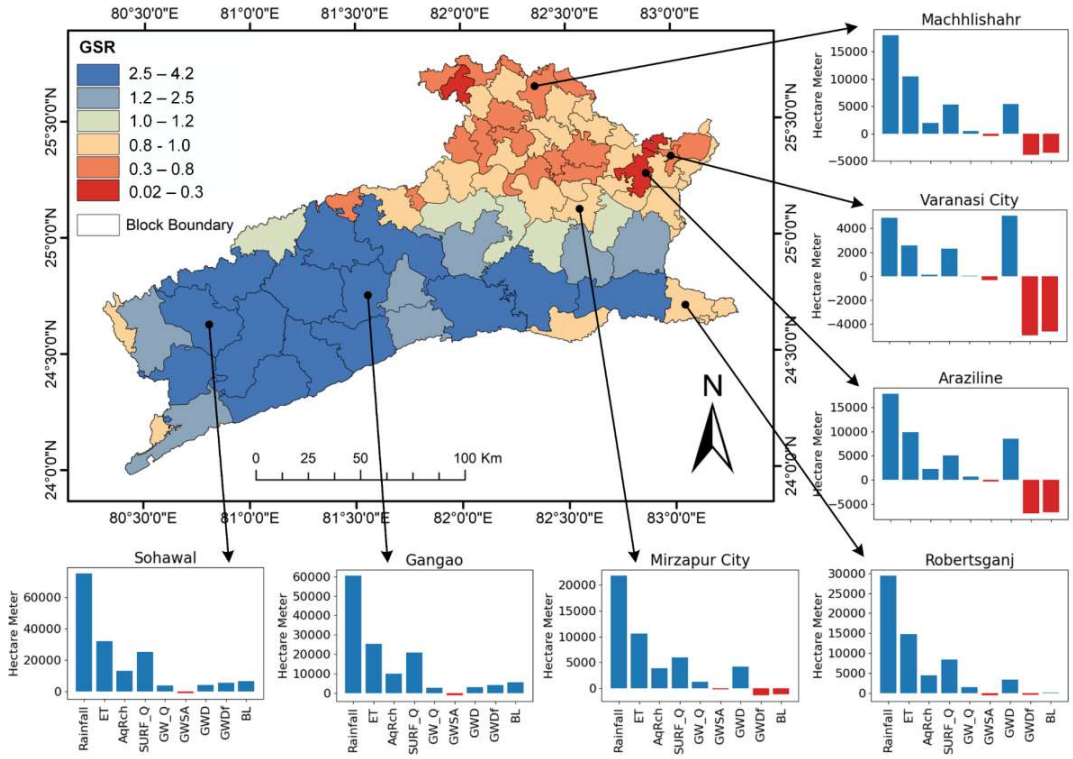


***Figure 4.13****.The GSR values in the study area and the annual average SW and GW budget of some blocks (2001-2013). chart (ET- Evapotranspiration, AqRch- Net recharge to the aquifer, SURF_Q- Surface runoff to the streams, GWSA- GWS Anomalies (-ve means decrease), GWD- total GW extraction, GWDf- GW deficiency (-ve means blocks are losing more GW than recharged and vice-versa) and BL- Boundary leakage (+ve means that block has surplus GW and vice-versa)*

## 4.6 SUMMARY

The study presents a novel methodology for the downscaling of GRACE-Terrestrial Water Storage Anomalies (GRACE-TWSA) to ascertain granular GW Storage (GWS) values. Initially, GRACE-TWSA data was refined to a finer scale using the Global Land Data Assimilation System (GLDAS) coupled with Artificial Neural Network 1 (ANN1) to amend biases inherent in GLDAS-Terrestrial Water Storage (TWS) estimations. Subsequently, the refined GWS data at the GLDAS scale underwent further downscaling to the Hydrologic Response Unit (HRU) scale leveraging Artificial Neural Network 2

(ANN2), which employed nine HRU variables exhibiting strong correlations as predictive factors. Furthermore, an analysis was conducted to ascertain the volumetric budget concerning pivotal SW and GW parameters, identifying GW deficiencies across distinct blocks within the study area.

The efficacy of the ANN model in the downscaling operation, with HRU variables serving as predictors, was deemed satisfactory. These HRU variables demonstrated a robust correlation with GWS. Such a correlation, alongside the observed GW levels' alignment with the refined GWS, facilitated an accurate determination of specific yield.

The study's findings indicated a decremental trend in GW storage within the Gangetic Plain, ranging from -1.4 mm to -6.9 mm annually from 2001 to 2014. Water budgeting within the designated area suggested prevalent water stress among most blocks within the Gangetic Plain, necessitating interventions to augment natural recharge.

This investigation leverages GRACE data to propose an innovative approach toward subbasin-scale SW and GW management. The methodology promises to supersede traditional GW modeling techniques for the detailed assessment of GW budgets and trends, which are often laborious within the realm of integrated water resource management. Integrating refined GWS and SWAT outputs is anticipated to yield a more precise calculation of hydrological parameters on a basin-wise scale.

***